Journal of The Electrochemical Society, **163** (2) A67-A74 (2016)
0013-4651/2016/163(2)/A67/8/$33.00 © The Electrochemical Society

Elastic Properties of Alkali Superionic Conductor Electrolytes from First Principles Calculations

Zhi Deng, Zhenbin Wang, Iek-Heng Chu, Jian Luo, and Shyue Ping Ong*,z

Department of NanoEngineering, University of California San Diego, La Jolla, California 92093-0448, USA

In this work, we present a comprehensive investigation of the elastic properties (the full elastic tensor, bulk, shear and Young's moduli, and Poisson's ratio) of 23 well-known ceramic alkali superionic conductor electrolytes (SICEs) using first principles calculations. We find that the computed elastic moduli are in good agreement with experimental data (wherever available) and chemical bonding nature. The anion species and structural framework have a significant influence on the elastic properties, and the relative elastic moduli of the various classes of SICEs follow the order thiophosphate < antiperovskite < phosphate < NASICON < garnet < perovskite. Within the same framework structure, we observe that Na SICEs are softer than their Li analogs. We discuss the implications of these findings in the context of fabrication, battery operation, and enabling a Li metal anode. The data computed in this work will also serve as a useful reference for future experiments as well as theoretical modeling of SICEs for rechargeable alkali-ion batteries.
 [DOI: 10.1149/2.0061602jes]

Manuscript submitted August 31, 2015; revised manuscript received October 12, 2015. Published November 5, 2015.

Alkali (lithium and sodium) superionic conductors have garnered increasing interest in recent years as potential replacement electrolytes for alkali-ion batteries.[1–9] The electrolyte in today's rechargeable alkali-ion batteries typically comprises a mixture of organic solvents (e.g., 1:1 ethylene carbonate and dimethyl carbonate) with an alkali salt (e.g., $Li/NaPF_6$) added for ionic conductivity. Such electrolytes are flammable and have limited electrochemical windows of up to 4.5 V.[10] Ceramic alkali superionic conductor electrolytes (SICEs), on the other hand, are non-flammable and can potentially have wider electrochemical windows. An all-solid-state rechargeable alkali-ion battery based on such a solid electrolyte would therefore represent a significant leap in safety and energy density.

The development of novel SICEs has thus far been mostly focused on the alkali ionic conductivity as the key design parameter, and there have been significant successes in this aspect. State-of-the-art sulfide SICEs such as $Li_{10}GeP_2S_{12}$ (LGPS) and $Li_7P_3S_{11}$[3,6,11–15] have alkali conductivities that rival those of liquid electrolytes (~ 10 mS/cm),[16] and oxide SICEs such as NASICON-type LATP (lithium aluminum titanium phosphate), perovskite-type LLTO (lithium lanthanum titanium oxide) and garnet-type LLZO ($Li_7La_3Zr_2O_{12}$), have alkali conductivities approximately one order of magnitude lower.[2,17–19]

However, less attention has been paid to the mechanical properties of SICEs, which can have a profound influence on the fabrication and performance of an all-solid-state rechargeable alkali-ion battery. For instance, a critical challenge in all-solid-state batteries is achieving and maintaining an intimate conformal contact with the electrodes during operation. Typical commercial cathodes (e.g., $LiCoO_2$, $LiMn_2O_4$ and $LiFePO_4$) and anodes (e.g., graphitic and hard carbons) exhibit chemical strains of up to 10% during electrochemical cycling.[20] The challenge is even greater with cutting edge Si anodes, which exhibit volume changes in excess of 300%.[21] The SICE must therefore be able to deform without the formation of cracks or pores to maintain the electrode/electrolyte interface during these volume changes, which would require "soft" SICEs that can acommodate large strains before failure. On the other hand, another potential application of SICEs is in enabling Li metal anodes by suppressing Li dendrite formation,[22] for which a SICE with high shear modulus and hardness would be more suitable.[23]

To the authors' knowledge, there have been only a few works exploring the mechanical properties of SICEs. Wolfenstine, Sakamoto and co-workers have reported on the Young's modulus and fracture toughness of polycrystalline Al-stabilized cubic LLZO garnet and LLTO perovskite.[24–26] Jackman et al. also characterized Young's modulus and fracture toughness of LATP.[27] In general, all these oxides exhibit relatively high Young's moduli (100-200 GPa) and fracture toughnesses of $\sim 1\,\mathrm{MPa}\sqrt{\mathrm{m}}$. In the sulfide chemistry, Sakuda et al. measured the Young's modulus of $Li_2S - P_2S_5$ glass electrolyte, which is tunable by its composition within the range of $18 \sim 25$ GPa.[28]

A common limitation of these experimental studies is that only the overall Young's modulus, Poisson's ratio and fracture toughness are measured. In rechargeable battery applications, the stresses/strains developed during operation are often anisotropic, requiring knowledge of the full elastic tensor. The full elastic tensor is also useful for understanding the development of internal stress fields during fabrication, which can often have a critical impact on final reliability and performance of the device. Another potential issue is that the measured values (which are mainly for polycrystalline samples) are highly dependent on various factors such as moisture, porosity and microstructure, and the presence of secondary phases.[24,26,27,29] Some chemistries are also inherently more challenging to handle experimentally, such as the sulfides which are sensitive to moisture and air.

First principles calculations based on density functional theory (DFT) can therefore be an invaluable complement to experiments in characterizing the intrinsic elastic properties (including the full elastic tensor) of SICEs. An example is the work of Wang et al., who calculated the elastic properties of the solid electrolyte LGPS from first principles calculations.[30] However, data on most SICEs are still lacking.

In this work, we perform a comprehensive investigation of the elastic properties of 23 well-known ceramic alkali SICEs using first principles calculations. We will provide an assessment of the accuracy of three exchange-correlation functionals - the Perdew-Burke-Ernzerhof (PBE),[31] PBE revised for solids (PBEsol)[32] generalized gradient approximation functionals and the van der Waals (vdW) density functional with opt88 exchange (optB88-vdW)[33] - in predicting elastic properties. We report the calculated full elastic tensors and other derived elastic properties (e.g., bulk, shear and Young's modulus, Poisson's ratio, etc.) of these well-known SICEs, and discuss observed trends with structure and chemistry. We will discuss the implications of the computed elastic properties for SICE design. The data compiled in this work will also serve as a useful reference for future experiments as well as theoretical battery models.[20,34]

SICE Selection

We have selected 23 well known Li-ion and Na-ion SICEs in a broad range of structures and chemistries for our study. It should be noted that a common strategy in optimizing many SICEs is through the formation of solid solutions or the introduction of dopants. For the purposes of this work, we will limit our investigations to the elastic properties of end members or undoped structures, which should nonetheless be representative of entire classes of materials. A further desired outcome of this study is to ascertain the effect of cation and anion chemistry on elastic properties. Where possible, we have

*Electrochemical Society Active Member.
zE-mail: ongsp@eng.ucsd.edu

included SICEs in both Li-ion and Na-ion chemistry and different anion chemistries if they are experimentally known.

The studied SICEs are as follows:

1. NAtrium SuperIonic CONductor (NASICON). The term NAtrium SuperIonic CONductor (NASICON) refers to a family of materials with general formula $AM(XO_4)_3$ (A: Li or Na, M: transition metal, X: P or Si), of which the framework structures consist of MO_6 octahedra and P/SiO_4 tetrahedra sharing common corners.[35,36] Among the huge family, the solid solution $Na_{1+x}Zr_2P_{3-x}Si_xO_{12}$ and Al doped $LiTi2(PO_4)_3$ (LATP) are two well-known alkali SICEs. We included end member $NaZr_2(PO_4)_3$ and undoped $LiT_2(PO_4)_3$ in this study. Both materials adopt a rhombohedral structure with space group $R\bar{3}c$.
2. Phosphate. Though $\gamma - Li_3PO_4$ is not a good SICE, it is still of great fundamental interest for two reasons. Firstly, the LIthium SuperIonic CONductor (LISICON) is a solid solution of two γ-Li_3PO_4 type of materials (e.g., Li_4GeO_4).[37,38] Also, the well-known glass electrolyte for thin-film Li-ion batteries, LIPON, is essentially N incorporated amorphous Li_3PO_4.[4,39]
3. LLTO Perovskite. The lithium lanthanum titanium oxides (LLTO) have a general formula of $Li_{3x}La_{2/3-x}TiO_3$ ($0 \leq x \leq 0.16$). They adopt perovskite structure with A-site deficiency. LLTO are of interest as SICE because of their high bulk ionic conductivity (1 mS/cm at room temperature).[18] Though the stoichiometry of LLTO is highly tunable, we only selected two compositions ($Li_{1/2}La_{1/2}TiO_3$ and $Li_{1/8}La_{5/8}TiO_3$) to represent this entire class of SICEs. For both compositions, we chose the ordered structures with lowest DFT energies found in the Materials Project[40] database.
4. Garnet. The ionic conduction in garnet-type structure $Li_5La_3M_2O_{12}$ (M: Ta or Nb, $Ia\bar{3}d$ space group) was first reported by the Weppner group.[41] Later, the same group reported $Li_7La_3Zr_2O_{12}$ (LLZO) with enhanced ionic conductivity to 0.4 mS/cm at room temperature.[19] The LLZO garnet is particularly attractive due to its excellent stability against lithium metal anode.[5] LLZO exists in two forms - a disordered cubic ($Ia\bar{3}d$ space group) form with higher conductivity[19] and an ordered tetragonal ($I4_1/acd$ space group) form with lower conductivity.[42] In this study, we have included the tetragonal ordered form of LLZO and the cubic $Li_5La_3M_2O_{12}$ (M: Ta or Nb).
5. Antiperovskite. The antiperovskites with general formula A_3OX (A: Li or Na, X: Cl or Br) are a recently discovered class of SICEs, with potential applications in both Li-ion and Na-ion chemistries.[43–47] We have included all ternary antiperovskites formed by the Li^+ and Na^+ cations and the Br^- and Cl^- anions, i.e., Li_3OCl, Li_3OBr, Na_3OCl and Na_3OBr, in this study.
6. Thiophosphate. The thiophosphates include a variety of materials, typically characterized by the presence of PS_4^{3-} tetrahedra (including condensed thiophosphates such as $P_2S_7^{4-}$), and P can partially be replaced by Ge, Si, Sn, etc.
   (a) Li_3PS_4. Isostructual with γ-Li_3PO_4, β-Li_3PS_4 is one of the end members of thio-LISICON solid solution $Li_{4-x}Ge_{1-x}P_xS_4$.[48] Nanoporous β-Li_3PS_4 shows significant improvement in ionic conductivity ($\sim$ 0.1 mS/cm) compared with its bulk form and γ-Li_3PS_4.[49] For calculating elastic properties of β-Li_3PS_4, between two types of symmetrically distinct partial occupied Li sites (Wycoff symbols: 4*b* and 4*c*), we assume that only 4*b* sites are fully occupied. Besides β-Li_3PS_4, we also have included the ordered γ-Li_3PS_4 structure (space group $Pmn2_1$) in this study for comparison.
   (b) $Li_{10}GeP_2S_{12}$. The recently reported $Li_{10}GeP_2S_{12}$ (LGPS) with space group $P4_2/nmc$ has one of the highest room temperature ionic conductivity (12 mS/cm) of known SICEs.[6,11] The Sn and Si analogs have also been predicted from first principles computations[12] to have similar ionic conductivity and were subsequently synthesized.[13,14] For our calculations, we use the ordered structures of all the three materials from previous DFT studies.[11,12] To preserve the tetragonal symmetry, we use the ordered structures with space group $P4_2/mc$.
   (c) $Li_7P_3S_{11}$. Crystallized from $Li_2S - P_2S_5$ glass, $Li_7P_3S_{11}$ has a triclinic structure with space group $P\bar{1}$. The framework structure contains PS_4 tetrahedra and P_2S_7 ditetrahedra.[50] $Li_7P_3S_{11}$ has the highest ionic conductivity (17 mS/cm) at room temperature reported to-date.[15]
   (d) Argyrodite Li_6PS_5X. The high Li-ion mobility in argyrodite Li_6PS_5X (X: Cl, Br, I) with space group $F\bar{4}3m$ was first reported by Deiseroth et al.[51] Argyrodites show ionic conductivity $\sim$ 1 mS/cm at room temperature in all-solid-state batteries.[52–54] In the argyrodite structures, Li-ions are randomly distributed in two types of sites. One of the sites (Wycoff symbol: 24*g*) is located at the center of a S_3 triangle with occupancy of 0.26, with two neighboring 48*h* sites with occupancy of 0.37. For this work, we assume that only the 24*g* sites are occupied.
   (e) Na_3PS_4. The cubic Na_3PS_4 was reported by Hayashi et al. with ionic conductivity $\sim$ 0.2 mS/cm at room temperature.[8] Compared with the previously known tetragonal Na_3PS_4 with lower ionic conductivity, the cubic phase is believed to be a high temperature phase with $I\bar{4}3m$ space group.[55] Similar as the argyrodite structures, two types of Na sites are available in cubic Na_3PS_4. The 6*b* Na sites sit on either face-centered or edge-centered positions with occupancy of 0.8, while the 12*d* Na sites with occupancy of 0.1 are found between two 6*b* sites. To obtain an ordered structure, we assume that only the 6b sites are occupied.

Methods

All spin-polarized calculations were performed using the Vienna ab initio simulation package (VASP) with the projector-augmented wave (PAW) method.[56,57] The cutoff for plane wave basis set was 520 eV and the electronic energy convergence was 10^{-6} eV. Structures were fully relaxed until the residual force on each atom was smaller than 0.01 eV/Å. The Brillouin-zone was sampled with a *k*-point density of 1000 per reciprocal atom. We used three different exchange-correlation functionals (PBE, PBEsol, optB88-vdW) to calculate the elastic constants. As the bulk moduli is quite sensitive to the lattice constant, the PBEsol functional was selected as it has been shown to be more accurate than PBE in reproducing lattice constants.[32] The optB88-vdW functional was chosen to account for van de Waals (vdW) interactions, which may be important in non-closed-packed structures.[58]

Recently, the Materials Project[40] has computed the elastic constants of inorganic compounds using an internally-developed code.[59] In this work, the elastic tensor, C_{ij} was calculated by performing six finite distortion of the lattice with the displacement of ± 0.015 Å and then fitted from the strain-stress relationship[60] implemented in VASP. We tested this approach against the data published in the Materials Project for LiH, Li_2O, Na_2O, CaS, MgO, Ga_2O_3, AlN, $BaZrO_3$, SrLiP, Sr_4Si_4Ru, and the results are in excellent agreement. The elastic moduli, such as bulk modulus B, shear modulus G and Young's modulus E were then derived based on the Voigt-Reuss-Hill (VRH) approximation.[61]

In the Voigt approximation, the elastic tensor, C_{ij} is predicted based on uniform strain, giving the upper limit of the bulk modulus B and shear modulus G.

$$B_V = \frac{(C_{11} + C_{22} + C_{33}) + 2(C_{12} + C_{23} + C_{31})}{9}, \quad [1]$$

$$G_V = \frac{(C_{11} + C_{22} + C_{33}) - (C_{12} + C_{23} + C_{31}) + 3(C_{44} + C_{55} + C_{66})}{15}. \quad [2]$$

In the Reuss approximation, the compliance tensor, s_{ij} is based on uniform stress, leading the lower boundary limit.

$$B_R = \frac{1}{(s_{11} + s_{22} + s_{33}) + 2(s_{12} + s_{23} + s_{31})}, \quad [3]$$

$$G_R = \frac{15}{4(s_{11} + s_{22} + s_{33}) - 4(s_{12} + s_{23} + s_{31}) + 3(s_{44} + s_{55} + s_{66})}, \quad [4]$$

where, the compliance tensor s_{ij} is described by

$$s_{ij} = C_{ij}^{-1}. \quad [5]$$

In Hill approximation, the arithmetic average of the Voigt and Reuss boundary limits is given by the following equations

$$B = \frac{B_V + B_R}{2}, \quad [6]$$

$$G = \frac{G_V + G_R}{2}. \quad [7]$$

In addition, Young's moduli E and Poisson's ration ν can be calculated by

$$E = \frac{9BG}{(3B + G)}, \quad [8]$$

$$\nu = \frac{(3B - 2G)}{2(3B + G)}. \quad [9]$$

We also applied the Born elastic stability criterion[62,63] to each of the systems studied to check if they were mechanically stable under zero pressure. This criterion in the harmonic approximation states that for a mechanically stable compound, the relevant elastic tensor must be positive definite, i.e., all its eigenvalues must be positive. The calculated elastic tensors for all systems studied in this work satisfy the Born criterion, regardless of the exchange-correlation functionals adopted.

All analyses in this work were performed using the Python Materials Genomics (pymatgen) materials analysis library.[64]

Results

Performance of various DFT functionals.— To assess the accuracy of various DFT functionals for the computation of elastic properties, we calculated the elastic properties of Li_2S, Li_2O and Na_2S using the PBE, PBEsol and optB88-vdW functionals, presented in Table I. These three materials were chosen based on the availability of experimental data on the full elastic tensors, as well as for their representativeness of the chemistries of interest in SICEs, which includes both lithium and sodium oxide and sulfides.

We observe that the standard PBE functional leads to lattice parameters that are somewhat larger than the experimental values ($\sim 0.5 - 1.1\%$), and the computed elastic constants and moduli are correspondingly smaller. This is consistent with the well-known tendency for PBE to underbind.[32] The PBEsol and optB88-vdW functionals both correct this tendency, leading to lattice constants and elastic moduli that are much closer to the experimental values. We still observe a relatively large difference ($\sim 53\%$) between the computed and experimentally measured elastic constants and moduli for Na_2S. We believe that this is likely due to experimental error, given that Na_2S is highly moisture and air sensitive (and any degradation of the material can have a significant impact on measured elastic properties) and the experimental data was reported in 1977. Overall, we find all three functionals to reproduce the expected trend of $Na_2S < Li_2S \ll Li_2O$ in the elastic constants and moduli.

We also tested the three functionals against a small set of SICEs whose bulk (B), shear (G) and Young's (E) modulus and Poisson's ratio (ν) have been previously determined (the full elastic tensors are not available experimentally). Table II summarizes the experimental and the calculated B, G, E and ν of three electrolyte materials using

Table I. Calculated lattice parameter (a_0), elastic tensor (C_{ij}), bulk modulus (B), shear modulus (G), Young's modulus (E) and Poisson's ratio (ν) for Li_2S ($Fm\bar{3}m$), Li_2O ($Fm\bar{3}m$), and Na_2S ($Fm\bar{3}m$) with the PBE, PBEsol and optB88-vdW functionals.

Material	Method	a_0 (Å)	C_{11} (GPa)	C_{12} (GPa)	C_{44} (GPa)	B (GPa)	G (GPa)	E (GPa)	ν
	PBE	5.721	83.6	18.9	33.7	40.4	33.2	78.2	0.18
		(−0.56%)	(12.37%)	(9.57%)	(−5.64%)	(11.60%)	-	-	-
	PBEsol	5.663	87.2	21.2	35.4	43.2	34.4	81.6	0.19
		(0.46%)	(8.60%)	(−1.44%)	(−10.97%)	(5.47%)	-	-	-
Li_2S	optB88-vdW	5.693	88.0	20.9	36.1	43.2	35.1	82.6	0.18
		(−0.07%)	(7.76%)	(0%)	(−13.17%)	(5.47%)	-	-	-
	Exp.[65]	5.689	95.4	20.9	31.9	45.7	-	-	-
	PBE	4.656	198.6	18.8	58.6	78.7	69.6	161.3	0.16
		(−1.09%)	(1.68%)	(12.56%)	(0.17%)	(3.67%)	-	-	-
	PBEsol	4.596	208.7	21.5	61.1	83.9	72.5	169.0	0.16
		(0.22%)	(−3.32%)	(0%)	(−4.09%)	(−2.69%)	-	-	-
Li_2O	optB88-vdW	4.636	207.0	25.4	62.8	85.8	72.8	170.3	0.17
		(−0.65%)	(−2.48%)	(−18.14%)	(−6.98%)	(−5.02%)	-	-	-
	Exp.[66]	4.606	202	21.5	58.7	81.7	69.8	162.9	0.17
	PBE	6.571	54.3	15.5	17.1	28.4	18.0	44.5	0.24
		(−0.52%)	(32.96%)	(53.03%)	(18.57%)	(42.04%)	-	-	-
	PBEsol	6.510	57.0	17.0	17.6	30.3	18.5	46.2	0.25
		(0.41%)	(29.64%)	(48.48%)	(16.19%)	(38.16%)	-	-	-
Na_2S	optB88-vdW	6.521	55.8	17.2	18.5	30.0	18.8	46.7	0.24
		(0.24%)	(31.11%)	(47.88%)	(11.9%)	(38.78%)	-	-	-
	Exp.[67,68]	6.537	81	33	21	49	-	-	-

[65]Lattice constants and elastic tensors measured at 10 K and 15 K, respectively.
[66]Lattice constant, elastic tensor and moduli measured at 293 K.
[67,68]Elastic tensors measured at 30 K.
Values in parentheses denote percentage error from experimental values.

Table II. Calculated bulk modulus (B, in GPa), shear modulus (G, in GPa), Young's modulus (E, in GPa) and Poisson's ratio (ν) for t-$Li_7La_3Zr_2O_{12}$ LLZO garnet, $Li_{1/2}La_{1/2}TiO_3$ LLTO perovskite and $LiTi_2(PO_4)_3$ LTP NASICON with the PBE, PBEsol and optB88-vdW exchange-correlation functionals.

Material	Method	B	G	E	ν
t-$Li_7La_3Zr_2O_{12}$	PBE	116.7	63.7	161.7	0.27
	PBEsol	127.4	68.9	175.1	0.27
	optB88-vdW	150.1	75.0	192.9	0.29
	Exp.[24]	102.8	59.6	149.8	0.26
$Li_{1/2}La_{1/2}TiO_3$	PBE	170.8	102.2	255.6	0.25
	PBEsol	183.5	104.0	262.4	0.26
	optB88-vdW	196.4	121.2	301.6	0.24
	Exp.[26]	133.3	80.0	200	0.25
$LiTi_2(PO_4)_3$	PBE	92.5	55.6	139.0	0.25
	PBEsol	95.0	57.6	143.7	0.25
	optB88-vdW	115.1	59.6	152.5	0.28
	Exp.[27]	-	-	115	-

[24]Al stablized cubic garnet $Li_{6.24}La_3Zr_2Al_{0.24}O_{11.98}$ with porosity 0.03, elastic moduli measured at room temperature.
[26]$Li_{0.33}La_{0.57}TiO_3$ obtained from solid-state procedure.
[27]High-purity, fine-grained $Li_{1.3}Al_{0.3}Ti_{1.7}(PO_4)_3$.

different exchange-correlation functionals. Similar to the previous test cases, the elastic moduli calculated with PBE are the smallest, while the optB88-vdW functional yields larger elastic moduli than PBEsol. For all three materials, the elastic moduli from all functionals are significantly higher than the values reported experimentally.[24,26,27] This difference can be attributed to a variety of factors. For example, the samples for characterization in experiments are all polycrystalline with finite grain size as well as porosity whereas they are modeled as infinite single crystals in plane-wave DFT. This can make a huge difference as in experiments, the elastic moduli of samples with different grain sizes or porosities vary.[24,26,27] The compositions used in our study are not exactly the same as experiments. In particular, the garnet $Li_7La_3Zr_2O_{12}$ studied in this work is the tetragonal form, while the reported experimental value is for the Al-stabilized cubic form. In fact, the elastic moduli for the cubic $Li_5La_3Ta_2O_{12}$ and $Li_5La_3Nb_2O_{12}$ are much closer to the experimentally reported values (see next section). Moreover, the DFT calculations are performed at 0 K, while experimental measurements are usually carried out at close to room temperature. Nevertheless, the trends in the elastic moduli are reproduced well with all three functionals.

Overall, our assessment is that the PBEsol functional is an excellent choice for the study of the elastic properties of SICEs, given that its much higher accuracy in reproducing the elastic constants of our tests systems compared to standard PBE.

Elastic properties of SICEs.— In Table III, we tabulate the elastic tensor, bulk (B), shear (G) and Young's (E) modulus and Poisson's ratio (ν) of each SICE studied in this work calculated using the PBEsol functional. We have also provided the PBE and optB88-vdW results in the Supplementary Information. To facilitate interpretation of the results, we have plotted the shear modulus (G) against the bulk

Table III. Calculated full elastic tensor (C_{ij}), bulk modulus (B), shear modulus (G), Young's modulus (E), Poisson's ratio (ν) and Pugh's ratio (G/B) using the PBEsol functional.

Formula	Space group	C_{ij} (GPa)	Number of independent C_{ij}	B (GPa)	G (GPa)	E (GPa)	ν	G/B
		NASICON						
$LiTi_2(PO_4)_3$	$R\bar{3}c$	$\begin{bmatrix} 226.0 & 86.7 & 43.9 & 7.9 & 0.0 & 0.0 \\ 86.7 & 226.0 & 43.9 & -7.9 & 0.0 & 0.0 \\ 43.9 & 43.9 & 116.3 & 0.0 & 0.0 & 0.0 \\ 7.9 & -7.9 & 0.0 & 48.6 & 0.0 & 0.0 \\ 0.0 & 0.0 & 0.0 & 0.0 & 48.6 & 7.9 \\ 0.0 & 0.0 & 0.0 & 0.0 & 7.9 & 69.6 \end{bmatrix}$	6	95.0	57.6	143.7	0.25	0.61
$NaZr_2(PO_4)_3$	$R\bar{3}c$	$\begin{bmatrix} 175.2 & 77.7 & 51.9 & 9.4 & 0.0 & 0.0 \\ 77.7 & 175.2 & 51.9 & -9.4 & 0.0 & 0.0 \\ 51.9 & 51.9 & 102.4 & 0.0 & 0.0 & 0.0 \\ 9.4 & -9.4 & 0.0 & 53.2 & 0.0 & 0.0 \\ 0.0 & 0.0 & 0.0 & 0.0 & 53.2 & 9.4 \\ 0.0 & 0.0 & 0.0 & 0.0 & 9.4 & 48.7 \end{bmatrix}$	6	86.3	47.7	120.9	0.27	0.55
		Phosphate						
Li_3PO_4	$Pnma$	$\begin{bmatrix} 116.5 & 45.4 & 36.5 & 0.0 & 0.0 & 0.0 \\ 45.4 & 123.9 & 62.5 & 0.0 & 0.0 & 0.0 \\ 36.5 & 62.5 & 127.4 & 0.0 & 0.0 & 0.0 \\ 0.0 & 0.0 & 0.0 & 38.9 & 0.0 & 0.0 \\ 0.0 & 0.0 & 0.0 & 0.0 & 41.1 & 0.0 \\ 0.0 & 0.0 & 0.0 & 0.0 & 0.0 & 53.9 \end{bmatrix}$	9	72.5	40.9	103.4	0.26	0.56
		Perovskite						
$Li_{1/8}La_{5/8}TiO_3$	$Pmm2$	$\begin{bmatrix} 309.6 & 105.3 & 102.0 & 0.0 & 0.0 & 0.0 \\ 105.3 & 335.0 & 130.3 & 0.0 & 0.0 & 0.0 \\ 102.0 & 130.3 & 295.3 & 0.0 & 0.0 & 0.0 \\ 0.0 & 0.0 & 0.0 & 73.1 & 0.0 & 0.0 \\ 0.0 & 0.0 & 0.0 & 0.0 & 89.8 & 0.0 \\ 0.0 & 0.0 & 0.0 & 0.0 & 0.0 & 96.4 \end{bmatrix}$	9	179.0	91.2	233.9	0.28	0.51
$Li_{1/2}La_{1/2}TiO_3$	$P2/c$	$\begin{bmatrix} 354.2 & 112.8 & 88.4 & 0.0 & -0.0 & 0.0 \\ 112.8 & 360.4 & 92.1 & 0.0 & -0.1 & 0.0 \\ 88.4 & 92.1 & 351.4 & 0.0 & -0.1 & 0.0 \\ 0.0 & 0.0 & 0.0 & 97.0 & 0.0 & -1.9 \\ -0.0 & -0.1 & -0.1 & 0.0 & 98.2 & 0.0 \\ 0.0 & 0.0 & 0.0 & -1.9 & 0.0 & 77.4 \end{bmatrix}$	13	183.5	104.0	262.5	0.26	0.57

Table III. (***Continued.***)

Formula	Space group	C_{ij} (GPa)	Number of independent C_{ij}	B (GPa)	G (GPa)	E (GPa)	ν	G/B
		Garnet						
$Li_5La_3Nb_2O_{12}$	$Ia\bar{3}d$	176.7 78.6 78.6 0.0 0.0 0.0 78.6 176.7 78.6 0.0 0.0 0.0 78.6 78.6 176.7 0.0 0.0 0.0 0.0 0.0 0.0 58.9 0.0 0.0 0.0 0.0 0.0 0.0 58.9 0.0 0.0 0.0 0.0 0.0 0.0 58.9	3	111.3	54.8	141.1	0.29	0.49
$Li_5La_3Ta_2O_{12}$	$Ia\bar{3}d$	179.6 78.1 78.1 0.0 0.0 0.0 78.1 179.6 78.1 0.0 0.0 0.0 78.1 78.1 179.6 0.0 0.0 0.0 0.0 0.0 0.0 59.9 0.0 0.0 0.0 0.0 0.0 0.0 59.9 0.0 0.0 0.0 0.0 0.0 0.0 59.9	3	112.0	56.1	144.2	0.29	0.50
$Li_7La_3Zr_2O_{12}$	$I4_1/acd$	196.9 92.7 86.2 0.0 0.0 0.0 92.7 196.9 86.2 0.0 0.0 0.0 86.2 86.2 224.2 0.0 0.0 0.0 0.0 0.0 0.0 80.1 0.0 0.0 0.0 0.0 0.0 0.0 80.1 0.0 0.0 0.0 0.0 0.0 0.0 71.0	6	127.4	68.9	175.1	0.27	0.54
		Antiperovskite						
Li_3OCl	$Pm\bar{3}m$	102.9 32.1 32.1 0.0 0.0 0.0 32.1 102.9 32.1 0.0 0.0 0.0 32.1 32.1 102.9 0.0 0.0 0.0 0.0 0.0 0.0 46.1 0.0 0.0 0.0 0.0 0.0 0.0 46.1 0.0 0.0 0.0 0.0 0.0 0.0 46.1	3	55.7	41.5	99.7	0.20	0.74
Li_3OBr	$Pm\bar{3}m$	91.0 33.0 33.0 0.0 0.0 0.0 33.0 91.0 33.0 0.0 0.0 0.0 33.0 33.0 91.0 0.0 0.0 0.0 0.0 0.0 0.0 46.6 0.0 0.0 0.0 0.0 0.0 0.0 46.6 0.0 0.0 0.0 0.0 0.0 0.0 46.6	3	52.3	38.5	92.8	0.20	0.74
Na_3OBr	$Pm\bar{3}m$	70.0 16.0 16.0 0.0 0.0 0.0 16.0 70.0 16.0 0.0 0.0 0.0 16.0 16.0 70.0 0.0 0.0 0.0 0.0 0.0 0.0 21.5 0.0 0.0 0.0 0.0 0.0 0.0 21.5 0.0 0.0 0.0 0.0 0.0 0.0 21.5	3	34.0	23.6	57.4	0.22	0.69
Na_3OCl	$Pm\bar{3}m$	78.1 15.5 15.5 0.0 0.0 0.0 15.5 78.1 15.5 0.0 0.0 0.0 15.5 15.5 78.1 0.0 0.0 0.0 0.0 0.0 0.0 20.9 0.0 0.0 0.0 0.0 0.0 0.0 20.9 0.0 0.0 0.0 0.0 0.0 0.0 20.9	3	36.4	24.6	60.2	0.22	0.68
		Thiophosphate: Li_3PS_4						
Li_3PS_4	$Pnma$	32.1 10.9 19.7 0.0 0.0 0.0 10.9 38.1 17.4 0.0 0.0 0.0 19.7 17.4 51.8 0.0 0.0 0.0 0.0 0.0 0.0 10.5 0.0 0.0 0.0 0.0 0.0 0.0 9.5 0.0 0.0 0.0 0.0 0.0 0.0 13.7	9	23.3	11.4	29.5	0.29	0.49
Li_3PS_4	$Pmn2_1$	53.8 23.3 23.8 0.0 0.0 0.0 23.3 49.2 27.3 0.0 0.0 0.0 23.8 27.3 44.9 0.0 0.0 0.0 0.0 0.0 0.0 12.3 0.0 0.0 0.0 0.0 0.0 0.0 15.0 0.0 0.0 0.0 0.0 0.0 0.0 11.7	9	32.9	12.6	33.4	0.33	0.38
		Thiophosphate: $Li_{10}MP_2S_{12}$						
$Li_{10}GeP_2S_{12}$	$P4_2mc$	44.9 27.7 12.6 0.0 0.0 0.0 27.7 44.9 12.6 0.0 0.0 0.0 12.6 12.6 51.2 0.0 0.0 0.0 0.0 0.0 0.0 3.5 0.0 0.0 0.0 0.0 0.0 0.0 3.5 0.0 0.0 0.0 0.0 0.0 0.0 12.4	6	27.3	7.9	21.7	0.37	0.29

Table III. (***Continued.***)

Formula	Space group	C_{ij} (GPa)	Number of independent C_{ij}	B (GPa)	G (GPa)	E (GPa)	ν	G/B
$Li_{10}SiP_2S_{12}$	$P4_2mc$	45.7 28.2 13.2 0.0 0.0 0.0 28.2 45.7 13.2 0.0 0.0 0.0 13.2 13.2 50.4 0.0 0.0 0.0 0.0 0.0 0.0 5.2 0.0 0.0 0.0 0.0 0.0 0.0 5.2 0.0 0.0 0.0 0.0 0.0 0.0 12.2	6	27.8	9.2	24.8	0.35	0.33
$Li_{10}SnP_2S_{12}$	$P4_2mc$	39.0 26.3 8.5 0.0 0.0 0.0 26.3 39.0 8.5 0.0 0.0 0.0 8.5 8.5 47.7 0.0 0.0 0.0 0.0 0.0 0.0 9.4 0.0 0.0 0.0 0.0 0.0 0.0 9.4 0.0 0.0 0.0 0.0 0.0 0.0 14.5	6	23.5	11.2	29.1	0.29	0.48
		Thiophosphate: $Li_7P_3S_{11}$						
$Li_7P_3S_{11}$	$P\bar{1}$	31.8 19.2 18.5 1.1 −2.9 −0.4 19.2 26.0 20.7 −1.5 2.8 1.4 18.5 20.7 49.3 −1.7 −1.8 1.6 1.1 −1.5 −1.7 10.7 3.2 1.5 −2.9 2.8 −1.8 3.2 13.6 −2.5 −0.4 1.4 1.6 1.5 −2.5 9.1	21	23.9	8.1	21.9	0.35	0.34
		Thiophosphate: Argyrodite						
Li_6PS_5Cl	$F\bar{4}3m$	39.9 23.1 23.1 0.0 0.0 0.0 23.1 39.9 23.1 0.0 0.0 0.0 23.1 23.1 39.9 0.0 0.0 0.0 0.0 0.0 0.0 7.8 0.0 0.0 0.0 0.0 0.0 0.0 7.8 0.0 0.0 0.0 0.0 0.0 0.0 7.8	3	28.7	8.1	22.1	0.37	0.28
Li_6PS_5Br	$F\bar{4}3m$	40.9 23.0 23.0 0.0 0.0 0.0 23.0 40.9 23.0 0.0 0.0 0.0 23.0 23.0 40.9 0.0 0.0 0.0 0.0 0.0 0.0 9.6 0.0 0.0 0.0 0.0 0.0 0.0 9.6 0.0 0.0 0.0 0.0 0.0 0.0 9.6	3	29.0	9.3	25.3	0.35	0.32
Li_6PS_5I	$F\bar{4}3m$	43.6 23.0 23.0 0.0 0.0 0.0 23.0 43.6 23.0 0.0 0.0 0.0 23.0 23.0 43.6 0.0 0.0 0.0 0.0 0.0 0.0 11.9 0.0 0.0 0.0 0.0 0.0 0.0 11.9 0.0 0.0 0.0 0.0 0.0 0.0 11.9	3	29.9	11.3	30.0	0.33	0.38
		Thiophosphate: Na_3PS_4						
Na_3PS_4	$I\bar{4}3m$	42.2 11.1 11.1 0.0 0.0 0.0 11.1 42.2 11.1 0.0 0.0 0.0 11.1 11.1 42.2 0.0 0.0 0.0 0.0 0.0 0.0 11.7 0.0 0.0 0.0 0.0 0.0 0.0 11.7 0.0 0.0 0.0 0.0 0.0 0.0 11.7	3	21.5	13.1	32.6	0.25	0.61
Na_3PS_4	$P\bar{4}2_1c$	49.8 11.4 15.7 0.0 0.0 0.0 11.4 49.8 15.7 0.0 0.0 0.0 15.7 15.7 42.9 0.0 0.0 0.0 0.0 0.0 0.0 11.1 0.0 0.0 0.0 0.0 0.0 0.0 11.1 0.0 0.0 0.0 0.0 0.0 0.0 11.7	6	25.3	13.1	33.6	0.28	0.52

modulus (B) for all investigated SICEs in Figure 1. We may make the following observations from Table III and Figure 1:

1. Somewhat unsurprisingly, we find that the sulfide SICEs are predicted to have very small elastic moduli ($E < 50$ GPa, $B < 40$ GPa, $G < 20$ GPa) compared to the oxides.
2. The structure framework and anion chemistry are primary determinants of the elastic properties of SICEs. All similar chemistries tend to have similar elastic moduli. The relative elastic moduli follow the order of thiophosphate < antiperovskite < phosphate < NASICON < garnet < perovskite.
3. Among the oxides, the phosphate (PO_4) framework structures such as the NASICON and Li_3PO_4 have significantly lower elastic moduli than the garnet and perovskites.
4. Within the same structural chemistries, we find that the Na version of the SICE has smaller elastic moduli than the Li analog. For example, the calculated Young's modulus of the Na_3OX (X: Cl, Br) antiperovskites are approximately 50 GPa, while that of the Li_3OX are closer to 100 GPa. A similar trend is also observed for the NASICON-based structures $LiTi_2(PO_4)_3$ and $NaZr_2(PO_4)_3$. For the A_3PS_4 compounds, both polymorphs of Na_3PS_4 are predicted to have both a much smaller bulk modulus as well as a smaller shear modulus than the two polymorphs of Li_3PS_4. The

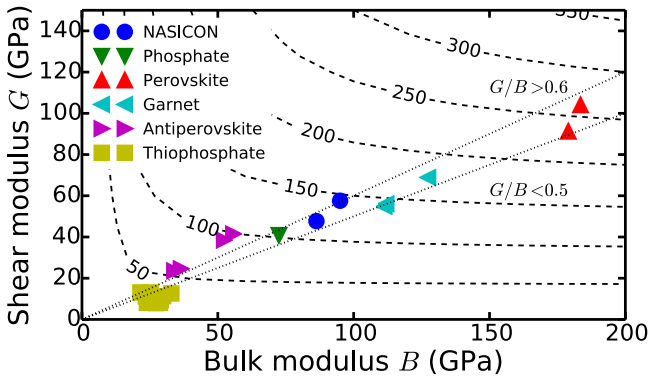

Figure 1. Plot of the shear modulus (G) vs bulk modulus (B) for all investigated SICEs calculated using the PBEsol functional. Dashed lines are the iso-Young's modulus lines in GPa. Two dotted lines correspond to $G/B = 0.5$ and $G/B = 0.6$.

overall Young's modulus of Na_3PS_4 is actually predicted to be similar to that of Li_3PS_4. It should be mentioned that the default step size of lattice displacement when calculating the elastic tensors produced negative C_{44} for cubic-Na_3PS_4, which can be attributed to "collapse" of the metastable cubic-Na_3PS_4. In this case, a very small strain ($\delta = 0.05\%$) was applied to evaluate its elastic tensor.

5. Among the garnet structures, we find that the tetragonal $Li_7La_3Zr_2O_{12}$ is predicted to have a much larger bulk, shear and Young's moduli than the cubic $Li_5La_3M_2O_{12}$ (M: Nb or Ta). As noted in the previous section, the calculated elastic moduli of the cubic $Li_5La_3M_2O_{12}$ are in fact extremely similar to the measured experimental values of cubic $Li_7La_3Zr_2O_{12}$. We hypothesize that the Li disorder and resulting structural symmetry have a substantial effect on the elastic moduli in this system. The transition metal cation (Nb/Ta) seems to have a relatively small effect on the elastic moduli, except in so far where aliovalent substitutions modify Li concentration and the structural symmetry.[69] In essence, we speculate that though the garnet framework comprises of La-O dodecahedra and Zr-O octahedra, strong Li-O interactions act as a "glue" that nonetheless have significant influence on elastic properties.
6. The Pugh's ratio, G/B[70] is commonly used to evaluate the brittleness of materials from elastic moduli. A larger G/B indicates that the material is more brittle. This criterion has been applied in ceramic materials in Li-ion batteries.[30,71,72] From our calculations, thiophosphates are the most ductile with lowest G/B ratio (< 0.5) among all the chemistries with a few exceptions (e.g., c-Na_3PS_4). For most oxides, the G/B ratio lies between 0.5 and 0.6, while the high G/B ratio in antiperovskites (~ 0.7) is an indication of their intrinsic brittle nature.

Discussion

This work is an attempt at addressing a critical knowledge gap - the lack of comprehensive data on the elastic properties of SICEs. The mechanical properties of SICEs can have a profound impact on the design and performance of all-solid-state batteries in many different aspects, including fabrication, battery operation and potentially enabling the use of a Li metal anode.

Fabrication.— One of the key requirements to fabricating a high-performing all-solid-state battery is achieving intimate conformal (pore and crack-free) contact of the SICE with the electrodes. Generally, such contact is harder to achieve in relatively "stiff" materials such as the LLTO and LLZO oxides, often requiring high-temperature sintering and densification techniques to achieve reasonable performance. Conversely, cold-press sintering is often sufficient to achieve a reasonably dense electrolyte with softer SICEs such the thiophosphates.[28] The residual stresses introduced by high-temperature fabrication routes, which depend on the magnitude as well as the anisotropy of the moduli, may make them prone to cracking and fracture. The full elastic modulus tensor, along with 3D orientation maps of polycrystals from simulation of electron backscattering measurements, can be used to access the development of non-uniform local residual stresses as a result of anisotropic elastic properties.

In cases where there are limited thermal budgets (e.g., certain components of all-solid-state batteries may be prone to evaporation or where inter-diffusion between different materials or components needs to be limited), thermal shocking resistance, which depends critically on the average modulus, becomes important. Also, as all-solid-state batteries have multiple layers of materials, any high-temperature processing will naturally result thermal stresses that depend on both the differential thermal expansion coefficients and moduli of all components, and high thermal stresses will likely result in delamination.

Battery operation.— During the charge and discharge of an alkali-ion battery, the electrode materials typically undergo significant lattice parameter changes that are usually anisotropic. For instance, the commercial $LiCoO_2$ cathode material undergoes large c lattice parameter changes of up to 2.6%, with the a and b lattice parameters experiencing much smaller changes of -0.39%.[73] Similarly, the $LiFePO_4$ olivine experiences significant changes in the a lattice parameter upon delithiation, sometimes with fracture occurring in the cathode material itself.[74] For good electrochemical performance, the SICE must be able to deform and maintain good conformal contact with the electrode throughout these lattice parameter changes. In this respect, "softer" SICEs would likely be able to accommodate these strains better while maintaining good electrode contact.

On the other hand, commercial batteries are often subject to mechanical abuse. A "harder" oxide SICEs would be better able to withstand mechanical shocks that can potentially perforate the battery and cause shorting.

Enabling the Li metal anode.— One of the holy grails in rechargeable Li-ion battery technology is enabling the use of Li metal instead of graphitic carbon as the anode. Such a Li metal anode would have a much higher theoretical specific capacity of 3860 mAh/g compared to 372 mAh/g for graphite anode.[22]

The key challenge in the use of Li metal anodes is the formation of dendrites during deposition. A model proposed by Monroe et al. demonstrated that a blocking layer with shear modulus twice that of lithium (4.2 GPa) can effectively suppress the growth of lithium dendrites.[23] Based on this simple model, all SICEs studied in this work would be able to mechanically block the growth of lithium dendrites. However, Nagao et al. observed that $Li_2S - P_2S_5$ glass electrolyte cracks at high current density (> 1 mA/cm^2), and lithium dendrites grow along the crack. This is attributed to the failure of SICE in accommodating the vast volume change due to the deposition of lithium.[75] Similar phenomena have also been observed in LLZO.[76] We may surmise that the stiffness of the SICE is less of a practical issue than achieving a dense, crack-free material.

A recurring theme in the above analyses is that from the purely mechanical perspective, "softer" SICEs would have the advantages of being able to achieve and maintain intimate contact with the electrodes more easily. Achieving (and maintaining) good contact in "stiff" oxide SICEs is largely an unresolved challenge today. A potential compromise is to use hybrid SICEs, where SICEs of different elastic moduli are combined into a composite electrolyte (assuming chemical compatibility). Yet another alternative is to incorporate a wetting liquid electrolyte with a "stiff" oxide electrolyte, with possibly a reduction in the safety benefits.

Conclusions

To conclude, we have investigated the elastic properties, including the full elastic tensor, bulk, shear and Young's moduli, and Poisson's

ratio of a broad spectrum of alkali superionic conductor electrolytes using first principles calculations. We find that the computed elastic constants are in good agreement with experimental data wherever available and chemical bonding nature. In general, we find that Na SICEs are somewhat softer than Li SICEs in the same structure, and the anion and structure type have a significant influence on the elastic properties. The data provided in this work would also provide a useful benchmark for future experimental investigations and computational modelings of SICEs for rechargeable alkali-ion battery applications.

Acknowledgments

This work was supported by the National Science Foundation's Designing Materials to Revolutionize and Engineer our Future (DMREF) program under Grant No. 1436976. Some of the computations in this work were performed using the Extreme Science and Engineering Discovery Environment (XSEDE), which is supported by National Science Foundation grant number ACI-1053575.

References

1. P. Knauth, *Solid State Ionics*, **180**, 911 (2009).
2. K. Takada, *Acta Mater.*, **61**, 759 (2013).
3. Y. S. Jung, D. Y. Oh, Y. J. Nam, and K. H. Park, *Isr. J. Chem.*, **55**, 472 (2015).
4. N. J. Dudney, *Mater. Sci. Eng. B*, **116**, 245 (2005).
5. M. Kotobuki, H. Munakata, K. Kanamura, Y. Sato, and T. Yoshida, *J. Electrochem. Soc.*, **157**, A1076 (2010).
6. N. Kamaya, K. Homma, Y. Yamakawa, M. Hirayama, R. Kanno, M. Yonemura, T. Kamiyama, Y. Kato, S. Hama, K. Kawamoto, and A. Mitsui, *Nat. Mater.*, **10**, 682 (2011).
7. M. Tatsumisago and A. Hayashi, *Solid State Ionics*, **225**, 342 (2012).
8. A. Hayashi, K. Noi, A. Sakuda, and M. Tatsumisago, *Nat. Commun.*, **3**, 856 (2012).
9. Y. Wang, W. D. Richards, S. P. Ong, L. J. Miara, J. C. Kim, Y. Mo, and G. Ceder, *Nat. Mater.*, **14**, 1026 (2015).
10. K. Xu, *Chem. Rev.*, **104**, 4303 (2004).
11. Y. Mo, S. P. Ong, and G. Ceder, *Chem. Mater.*, **24**, 15 (2012).
12. S. P. Ong, Y. Mo, W. D. Richards, L. Miara, H. S. Lee, and G. Ceder, *Energy Environ. Sci.*, **6**, 148 (2013).
13. P. Bron, S. Johansson, K. Zick, J. S. A. Der Günne, S. Dehnen, and B. Roling, *J. Am. Chem. Soc.*, **135**, 15694 (2013).
14. A. Kuhn, O. Gerbig, C. Zhu, F. Falkenberg, J. Maier, and B. V. Lotsch, *Phys. Chem. Chem. Phys.*, **16**, 14669 (2014).
15. Y. Seino, T. Ota, and K. Takada, *Energy Environ. Sci.*, **7**, 627 (2014).
16. K. Hayashi, Y. Nemoto, S.-i. Tobishima, and J.-i. Yamaki, *Electrochim. Acta*, **44**, 2337 (1999).
17. H. Aono, E. Sugimoto, Y. Sadaoka, N. Imanaka, and G.-Y. Adachi, *J. Electrochem. Soc.*, **136**, 590 (1989).
18. Y. Inaguma, C. Liquan, M. Itoh, T. Nakamura, T. Uchida, H. Ikuta, and M. Wakihara, *Solid State Commun.*, **86**, 689 (1993).
19. R. Murugan, V. Thangadurai, and W. Weppner, *Angew. Chemie Int. Ed.*, **46**, 7778 (2007).
20. W. H. Woodford, W. C. Carter, and Y.-M. Chiang, *Energy Environ. Sci.*, **5**, 8014 (2012).
21. H. Wu and Y. Cui, *Nano Today*, **7**, 414 (2012).
22. W. Xu, J. Wang, F. Ding, X. Chen, E. Nasybulin, Y. Zhang, and J.-G. Zhang, *Energy Environ. Sci.*, **7**, 513 (2014).
23. C. Monroe and J. Newman, *J. Electrochem. Soc.*, **152**, A396 (2005).
24. J. E. Ni, E. D. Case, J. S. Sakamoto, E. Rangasamy, and J. B. Wolfenstine, *J. Mater. Sci.*, **47**, 7978 (2012).
25. J. Wolfenstine, H. Jo, Y.-H. Cho, I. N. David, P. Askeland, E. D. Case, H. Kim, H. Choe, and J. Sakamoto, *Mater. Lett.*, **96**, 117 (2013).
26. Y.-H. Cho, J. Wolfenstine, E. Rangasamy, H. Kim, H. Choe, and J. Sakamoto, *J. Mater. Sci.*, **47**, 5970 (2012).
27. S. D. Jackman and R. A. Cutler, *J. Power Sources*, **218**, 65 (2012).
28. A. Sakuda, A. Hayashi, and M. Tatsumisago, *Sci. Rep.*, **3**, 2261 (2013).
29. R. M. Spriggs, *J. Am. Ceram. Soc.*, **44**, 628 (1961).
30. Z. Q. Wang, M. S. Wu, G. Liu, X. L. Lei, B. Xu, and C. Y. Ouyang, *Int. J. Electrochem. Sci.*, **9**, 562 (2014).
31. J. P. Perdew, K. Burke, and M. Ernzerhof, *Phys. Rev. Lett.*, **77**, 3865 (1996).
32. J. P. Perdew, A. Ruzsinszky, G. I. Csonka, O. A. Vydrov, G. E. Scuseria, L. A. Constantin, X. Zhou, and K. Burke, *Phys. Rev. Lett.*, **100**, 136406 (2007).
33. J. Klimeš, D. R. Bowler, and A. Michaelides, *J. Physics. Condens. Matter*, **22**, 022201 (2010).
34. W. H. Woodford, Y.-M. Chiang, and W. C. Carter, *J. Electrochem. Soc.*, **157**, A1052 (2010).
35. J. B. Goodenough, H. Y.-P. Hong, and J. A. Kafalas, *Mater. Res. Bull.*, **11**, 203 (1976).
36. H. Y.-P. Hong, *Mater. Res. Bull.*, **11**, 173 (1976).
37. H. Y.-P. Hong, *Mater. Res. Bull.*, **13**, 117 (1978).
38. J. Kuwano and A. R. West, *Mater. Res. Bull.*, **15**, 1661 (1980).
39. X. Yu, J. B. Bates, G. E. Jellison, and F. X. Hart, *J. Electrochem. Soc.*, **144**, 524 (1997).
40. A. Jain, S. P. Ong, G. Hautier, W. Chen, W. D. Richards, S. Dacek, S. Cholia, D. Gunter, D. Skinner, G. Ceder, and K. A. Persson, *APL Mater.*, **1**, 011002 (2013).
41. V. Thangadurai, H. Kaack, and W. J. F. Weppner, *J. Am. Ceram. Soc.*, **86**, 437 (2003).
42. J. Awaka, N. Kijima, H. Hayakawa, and J. Akimoto, *J. Solid State Chem.*, **182**, 2046 (2009).
43. Y. Zhao and L. L. Daemen, *J. Am. Chem. Soc.*, **134**, 15042 (2012).
44. Y. Zhang, Y. Zhao, and C. Chen, *Phys. Rev. B*, **87**, 134303 (2013).
45. A. Emly, E. Kioupakis, and A. Van der Ven, *Chem. Mater.*, **25**, 4663 (2013).
46. Z. Deng, B. Radhakrishnan, and S. P. Ong, *Chem. Mater.*, **27**, 3749 (2015).
47. Y. Wang, Q. Wang, Z. Liu, Z. Zhou, S. Li, J. Zhu, R. Zou, Y. Wang, J. Lin, and Y. Zhao, *J. Power Sources*, **293**, 735 (2015).
48. R. Kanno and M. Murayama, *J. Electrochem. Soc.*, **148**, A742 (2001).
49. Z. Liu, W. Fu, E. A. Payzant, X. Yu, Z. Wu, N. J. Dudney, J. Kiggans, K. Hong, A. J. Rondinone, and C. Liang, *J. Am. Chem. Soc.*, **135**, 975 (2013).
50. H. Yamane, M. Shibata, Y. Shimane, T. Junke, Y. Seino, S. Adams, K. Minami, A. Hayashi, and M. Tatsumisago, *Solid State Ionics*, **178**, 1163 (2007).
51. H. J. Deiseroth, S. T. Kong, H. Eckert, J. Vannahme, C. Reiner, T. Zaiß, and M. Schlosser, *Angew. Chemie Int. Ed.*, **47**, 755 (2008).
52. R. P. Rao and S. Adams, *Phys. Status Solidi*, **208**, 1804 (2011).
53. S. Boulineau, M. Courty, J.-M. Tarascon, and V. Viallet, *Solid State Ionics*, **221**, 1 (2012).
54. S. Boulineau, J.-M. Tarascon, J. B. Leriche, and V. Viallet, *Solid State Ionics*, **242**, 45 (2013).
55. N. Tanibata, K. Noi, A. Hayashi, N. Kitamura, Y. Idemoto, and M. Tatsumisago, *ChemElectroChem*, **1**, 1130 (2014).
56. G. Kresse and J. Furthmüller, *Phys. Rev. B*, **54**, 11169 (1996).
57. P. E. Blöchl, *Phys. Rev. B*, **50**, 17953 (1994).
58. J. Klimeš, D. R. Bowler, and A. Michaelides, *Phys. Rev. B*, **83**, 195131 (2011).
59. M. de Jong, W. Chen, T. Angsten, A. Jain, R. Notestine, A. Gamst, M. Sluiter, C. K. Ande, S. V. D. Zwaag, J. J. Plata, C. Toher, S. Curtarolo, G. Ceder, K. A. Persson, and M. Asta, *Sci. Data*, **2**, 150009 (2015).
60. Y. Le Page and P. Saxe, *Phys. Rev. B*, **65**, 104104 (2002).
61. R. Hill, *Proc. Phys. Soc. Sect. A*, **65**, 349 (2002).
62. M. Born, *Math. Proc. Cambridge Philos. Soc.*, **36**, 160 (1940).
63. F. Mouhat and F.-X. Coudert, *Phys. Rev. B*, **90**, 224104 (2014).
64. S. P. Ong, W. D. Richards, A. Jain, G. Hautier, M. Kocher, S. Cholia, D. Gunter, V. L. Chevrier, K. A. Persson, and G. Ceder, *Comput. Mater. Sci.*, **68**, 314 (2013).
65. W. Buehrer, F. Altorfer, J. Mesot, H. Bill, P. Carron, and H. G. Smith, *J. Phys. Condens. Matter*, **3**, 1055 (1991).
66. S. Hull, T. Farley, W. Hayes, and M. Hutchings, *J. Nucl. Mater.*, **160**, 125 (1988).
67. B. Bertheville, D. Low, H. Bill, and F. Kubel, *J. Phys. Chem. Solids*, **58**, 1569 (1997).
68. W. Buhrer and H. Bill, *Helv. Phys. Acta*, **50**, 431 (1977).
69. N. Bernstein, M. Johannes, and K. Hoang, *Phys. Rev. Lett.*, **109**, 205702 (2012).
70. S. Pugh, *Philos. Mag. Ser. 7*, **45**, 823 (1954).
71. S.-L. Shang, L. G. Hector, S. Shi, Y. Qi, Y. Wang, and Z.-K. Liu, *Acta Mater.*, **60**, 5204 (2012).
72. Y. Qi, L. G. Hector, C. James, and K. J. Kim, *J. Electrochem. Soc.*, **161**, F3010 (2014).
73. J. N. Reimers and J. R. Dahn, *J. Electrochem. Soc.*, **139**, 2091 (1992).
74. N. Meethong, H. Y. S. Huang, S. A. Speakman, W. C. Carter, and Y. M. Chiang, *Adv. Funct. Mater.*, **17**, 1115 (2007).
75. M. Nagao, A. Hayashi, M. Tatsumisago, T. Kanetsuku, T. Tsuda, and S. Kuwabata, *Phys. Chem. Chem. Phys.*, **15**, 18600 (2013).
76. Y. Ren, Y. Shen, Y. Lin, and C.-W. Nan, *Electrochem. commun.*, **57**, 27 (2015).